


Heat transport at boiling, near-critical conditions

Journal Article

Author(s):

Coumou, Dim; Driesner, Thomas; Heinrich, Christoph A. 

Publication date:

2008-09

Permanent link:

<https://doi.org/10.3929/ethz-b-000011132>

Rights / license:

In Copyright - Non-Commercial Use Permitted

Originally published in:

Geofluids 8(3), <https://doi.org/10.1111/j.1468-8123.2008.00218.x>

Heat transport at boiling, near-critical conditions

D. COUMOU, T. DRIESNER AND C. A. HEINRICH

Institute of Isotope Geochemistry and Mineral Resources, ETH Zuerich, Zuerich, Switzerland

ABSTRACT

Two-phase flow and near-critical phenomena are likely to enhance energy transport in high-temperature hydrothermal systems. We present a series of two-dimensional simulations of two-phase flow of pure water at near-critical conditions. The results show that at near-critical conditions, two-phase convection can be more efficient in transporting energy than single-phase convection. The highest heat fluxes are attained when two-phase heat-pipes form near the bottom boundary, recharging the root of the upflow zone and thereby enabling the formation of broad upflow regions. When the system becomes more vapor-dominated, it loses this ability, upflow zones become narrower and the energy efficiency drops to more moderate values.

Key words: CSMP++, multi-phase flow, near-critical phenomena, hydrothermal systems, heat-pipes

Received 28 April 2008; accepted 21 August 2008

Corresponding author: D. Coumou, Earth System Analysis, Potsdam Institute for Climate Impact Research (PIK), P.O. Box 601203, 14412 Potsdam, Germany.

Email: coumou@pik-potsdam.de. Tel: +49 331 288 2442. Fax: +49 331 288 2620.

Geofluids (2008) 8, 208–215

INTRODUCTION

The temperature- and pressure-dependence of thermodynamic and transport properties of water can substantially influence the onset, style and duration of thermal convection in porous media (Schubert & Straus 1977; Jupp & Schultz 2000, 2004). This effect becomes extreme near the critical point of water, where the thermal expansivity peaks and the kinematic viscosity exhibits a minimum, such that buoyancy forces are maximized and viscous drag forces are minimized. Together with a peak in heat capacity, this leads to very efficient energy-transport mechanisms (Norton & Knight 1977; Dunn & Hardee 1981; Ingebritsen & Hayba 1994), allowing hydrothermal systems to operate in a mode of maximum energy transport (Jupp & Schultz 2004).

It was recognized some decades ago that fluids in hydrothermal systems in various geological settings can reach temperature–pressure conditions near the fluid's critical point. For example, many black-smoker vent fluids are close to the critical points of water (22.1 MPa, 374°C) and seawater (29.8 MPa, 407°C) (Jupp & Schultz 2000; Von Damm *et al.* 2003). Similarly, the deeper parts of continental geothermal and magmatic-hydrothermal systems can encompass the near-critical region (Cathles 1977; Norton & Knight 1977; Straus & Schubert 1977; Inge-

britsen & Hayba 1994; Hayba & Ingebritsen 1997; Fournier 1999; Hurwitz *et al.* 2003; Heinrich *et al.* 2004). Numerical simulations that specifically studied the effect of near-critical convection in a geological context have been rare (Cox & Pruess 1990; Ingebritsen & Hayba 1994). Cox & Pruess (1990) attempted to reproduce an earlier experimental study of near-critical water convection (Dunn & Hardee 1981). Hayba & Ingebritsen (1997) studied convection in large hydrothermal systems around cooling plutons but did not carry out a detailed analysis of heat transfer. More recently, Jupp & Schultz (2000, 2004) found that the strong nonlinear variations in water properties in the supercritical region will give rise to local Rayleigh-instabilities and force convection to operate in the temperature–pressure regime where the properties of water change most strongly.

A second mechanism that allows very efficient heat transport is the 'heat-pipe'. Heat-pipes form if the pressure gradient in two-phase upflow zones settles between vapor-static and liquid-static, such that liquid flows downwards and vapor upwards. Energy is absorbed at the base of the heat-pipe and carried upward by the low-density, high-enthalpy vapor phase and released as latent heat of condensation at the top of the heat-pipe (Schubert & Straus 1979, 1980; McGuinness *et al.* 1993; McGuinness 1996, 1997; Bai *et al.* 2003). A detailed study of vapor- versus

liquid-dominated heat-pipes was presented by McGuinness *et al.* (1993) and McGuinness (1996, 1997). The relevance of heat-pipes in the context of mid-ocean ridge hydrothermal systems was discussed by Bai *et al.* (2003) and Seyfried *et al.* (2003).

Most of the studies mentioned above focused on various aspects of the convection process such as the conditions that lead to the onset of convection or the formation of a particular flow style. Schubert & Straus (1977) and Straus & Schubert (1977) stressed the outstanding importance of realistic fluid properties in obtaining realistic results and stated the need for further studies. Nevertheless, the efficiency of heat transport using realistic fluid properties has been addressed by relatively few studies, notably Cox & Pruess (1990), Ingebritsen & Hayba (1994) and Fontaine & Wilcock (2007). One reason for the limited number of studies is that numerical modeling of convection at near-critical conditions is challenging, due to the aforementioned extrema in fluid properties, the singularity in the equation of state at the critical point when expressed in terms of temperature and two-phase flow at subcritical conditions.

The efficiency of heat transport is commonly described by the Nusselt number (Nu), which is the transported energy divided by the energy transport by conduction only. Fontaine & Wilcock (2007) studied the efficiency of energy transport at supercritical conditions in open-top systems, in which fluids are allowed to flow undisturbed through the top of the model. They used nonlinear but still simplified fluid properties. For their specific model, they found Nu ranging from approximately 12 for low-permeability systems ($2.25 \times 10^{-15} \text{ m}^2$) to approximately 50 for a higher permeability of $1.12 \times 10^{-14} \text{ m}^2$. This shows that energy transport at supercritical conditions can be very efficient. Ingebritsen & Hayba (1994) showed that heat transfer by single-phase fluids close to the critical point itself can be even more efficient, reaching Nu of up to approximately 200. In order to create such large Nu , relatively large permeabilities (10^{-12} – 10^{-13} m^2) were required, leading to the conclusion that superconvection, i.e. convection with $Nu > 100$, is probably not very common in nature. However, their only two-phase simulation produced a substantially higher efficiency ($Nu \approx 500$), suggesting that near-critical two-phase processes can enhance heat transfer substantially. Intuitively, this makes sense, as the low density of the vapor phase enhances buoyancy forces that could reinforce convection, and the vapor's specific enthalpy is larger at subcritical pressures than at the critical point itself (Ingebritsen *et al.* 2006).

In this study, we investigate the effects of near-critical single- and two-phase flows in two dimensions. In contrast to Ingebritsen & Hayba (1994), we study the convection over larger domains, using model sizes appropriate for black-smoker hydrothermal systems. In contrast to Fontaine & Wilcock (2007), we allow for two-phase flow of

liquid and vapor in our simulations, allow for fully transient density variations and use the full rather than simplified water properties. The bottom boundary condition is set to constant temperature rather than constant heat flux, as this allows calculating the increased efficiency of energy transport due to convection as opposed to conduction only. We apply different top pressures, permeability and relative-permeability scenarios and present the simulation results in terms of Nu . The results show that very large Nu can be achieved, up to approximately 1000, but only under restricted conditions.

COMPUTATIONAL METHOD

We use the pressure-enthalpy-based multi-phase fluid-transport scheme of our numerical modeling code CSMP++, in which the following expressions for mass and energy conservation are solved (Coumou 2008):

$$\phi \frac{\partial[(S_l \rho_l + S_v \rho_v)]}{\partial t} = -\nabla(\mathbf{v}_l \rho_l) - \nabla(\mathbf{v}_v \rho_v) \quad (1)$$

$$\begin{aligned} \frac{\partial[(1-\phi)\rho_r h_r + \phi(S_l \rho_l h_l + S_v \rho_v h_v)]}{\partial t} \\ = -\nabla(\mathbf{v}_l \rho_l h_l) - \nabla(\mathbf{v}_v \rho_v h_v) - \nabla K \nabla T. \end{aligned} \quad (2)$$

Here, ϕ is the porosity, S volumetric saturation, ρ density, h specific enthalpy, K thermal conductivity and T temperature, and subscripts l , v and r stand for liquid, vapor and rock respectively. We assume that the volume flux \mathbf{v} can be described by the two-phase form of the Darcy equation (Ingebritsen *et al.* 2006):

$$\mathbf{v}_i = -\mathbf{k} \frac{k_{ri}}{\mu_i} [\nabla p - \rho_i \mathbf{g}] \quad i = \{l, v\}, \quad (3)$$

where \mathbf{k} is the intrinsic permeability, k_r the relative permeability, μ viscosity, p pressure and \mathbf{g} the acceleration due to gravity. In our approach, we assume that fluid and rock are in thermal equilibrium, capillary-pressure effects are negligible, the rock matrix is incompressible and that the fluid can be described by pure water (Haar *et al.* 1984).

We solve equations 1–3 on a rectangular two-dimensional $1500 \times 500 \text{ m}$ domain discretized with a total of approximately 21 000 triangular elements. The side boundaries were set to no flow and the bottom boundary to constant temperature and no flow. The top boundary was set to constant pressure values typical of marine hydrothermal systems. To allow hot fluids to vent, a mixed-energy boundary condition was applied at the top. In elements where the total volume flux ($\mathbf{v}_l + \mathbf{v}_v$) was upwards, the temperature gradient was set to zero to allow undisturbed venting of upwelling fluids (Jupp & Schultz 2000; Coumou *et al.* 2006). Elements where the total volume flux was downwards take in cold water. We vary

Table 1 List of simulations.

Simulation	k (m ²)	k_r	p_{top} (MPa)	T_{bottom} (°C)
1	5e-15	Linear	15	300
2	5e-15	Linear	15	350
3	5e-15	Linear	15	360
4	5e-15	Linear	15	370
5	5e-15	Linear	15	380
6	5e-15	Linear	15	400
7	5e-15	Linear	15	450
8	5e-15	Linear	15	600
9	5e-15	Linear	18	370
10	5e-15	Linear	18	380
11	5e-15	Linear	18	450
12	5e-15	Linear	18	700
13	5e-14	Linear	18	370
14	5e-14	Linear	18	380
15	5e-14	Linear	18	390
16	5e-15	Nonlinear	15	380
17	5e-15	Nonlinear	15	450
18	5e-15	Nonlinear	15	700
19	5e-15	Nonlinear	21	380
20	5e-15	Nonlinear	21	400
21	5e-15	Nonlinear	21	450
22	5e-15	Nonlinear	21	550
23	5e-15	Nonlinear	21	700

the temperature at the bottom boundary from 300 to 700°C and analyze energy transport through the top of the domain. In most simulation runs, we set the pressure at the top to 15 MPa, use linear relative permeability functions with residual saturations for liquid and vapor of 0.3 and 0 respectively, and invoke a homogeneous permeability of $5.0 \times 10^{-15} \text{ m}^2$. In successive simulation runs (Table 1), we vary the top pressure (to 18 and 21 MPa) and permeability (to $5.0 \times 10^{-14} \text{ m}^2$) and test nonlinear relative-permeability relations.

We present results in terms of the Nu . It should be noted that, in its general form, Nu is a scale- and geometry-dependent property, as the characteristic lengths of the various modes of heat transfer in a given process have to be taken into account. Here, we are interested in the overall enhancement of heat transfer through the top boundary due to advective transport. Hence, we take $Nu = Q/(K\Delta T/\Delta z)$, with Q being the horizontally averaged, advective plus conductive heat flux through the top boundary. This is divided by the steady-state conductive heat transfer for the system as the reference case. Following Hurwitz *et al.* (2003) and Ingebritsen *et al.* (2006), we take the advective contribution as $Q_{\text{adv}} = v_f \rho_f h_f$ where v_f is the vertical component of fluid flux across the top boundary at a given point. This expression is not strictly correct, as the specific enthalpy is not defined on an absolute scale but always relative to a reference state. In the case of the Haar–Gallagher–Kell equation of state for pure water (Haar *et al.* 1984) employed here, this is the enthalpy of the pure liquid at the triple point of water. For

systems where water intake is at low temperatures (i.e. close to the reference state) and outflow at high temperatures, errors resulting from using this expression are negligible. In other cases, care must be taken to properly compute the heat taken up by the fluid on its path through the system.

RESULTS

We can identify four basic convection types, which we will refer to as: (i) single-phase, (ii) two-phase heat-pipe, (iii) two-phase vapor-dominated and (iv) supercritical systems. Single-phase fluid flow occurs when bottom temperatures are set below the boiling temperature for near-bottom pressures (Table 1, simulations 1,2,3,9). Single-phase convection is characterized by relatively large aspect ratios (0.75–1.0), defined as the width of one convection cell divided by its height (Fig. 1). The efficiency in transporting energy is relatively low, with $Nu < 5$. The temperature of upwelling fluids drops substantially on their way up, as shown in the pressure–temperature diagram (Fig. 2).

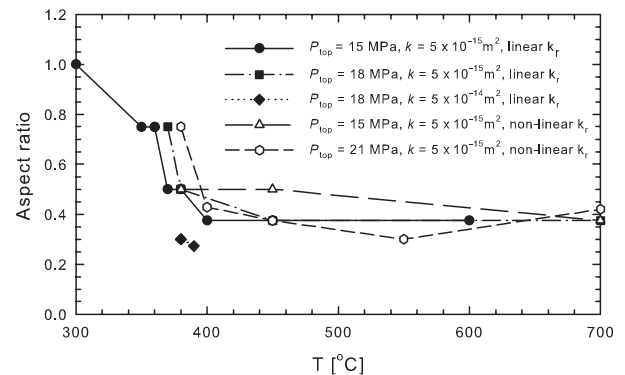


Fig. 1. Aspect ratio of convection cells as a function of bottom-boundary temperature for different top-boundary pressures, permeabilities and relative-permeability functions.

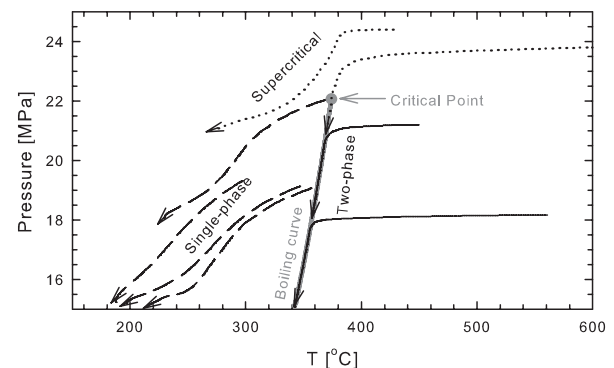


Fig. 2. Pressure–temperature paths of upflowing fluids for single-phase (dashed), two-phase (solid) or supercritical (dotted) simulation runs, relative to the boiling curve and critical point of pure water (solid grey).

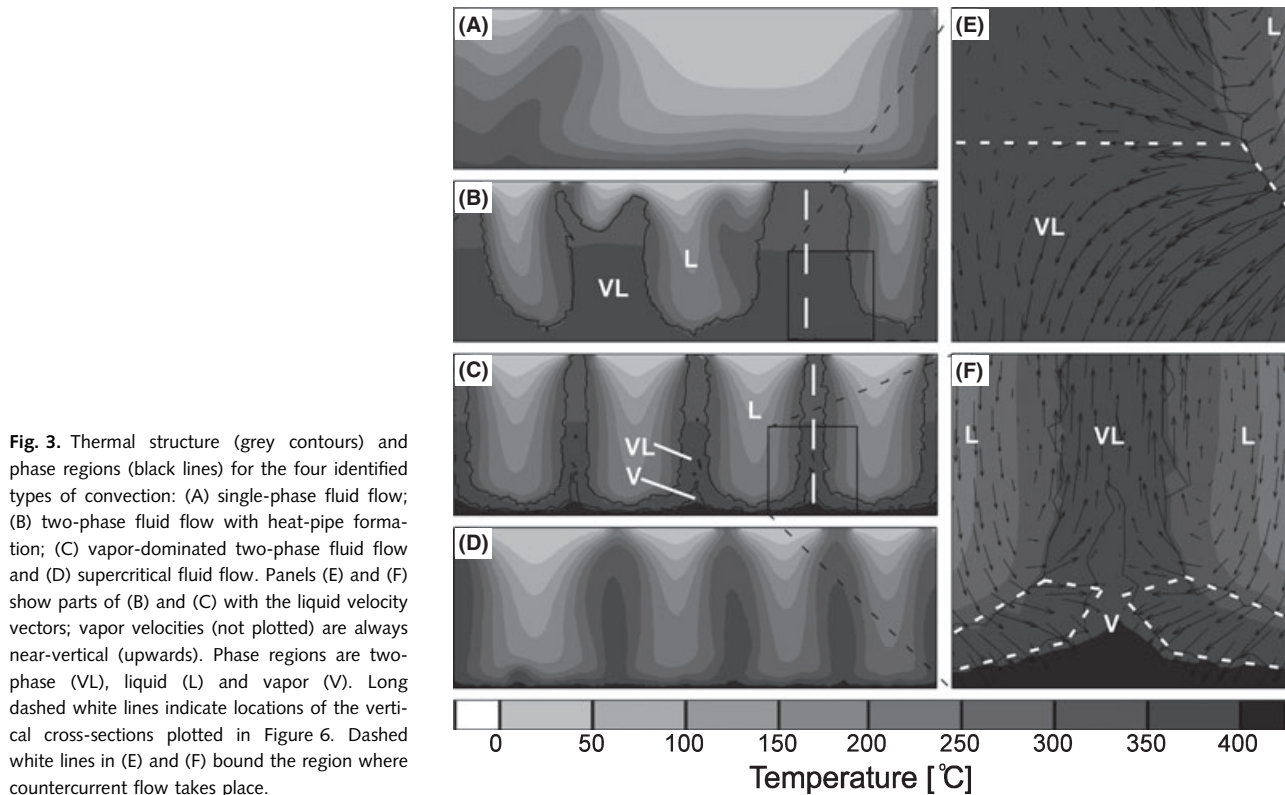


Fig. 3. Thermal structure (grey contours) and phase regions (black lines) for the four identified types of convection: (A) single-phase fluid flow; (B) two-phase fluid flow with heat-pipe formation; (C) vapor-dominated two-phase fluid flow and (D) supercritical fluid flow. Panels (E) and (F) show parts of (B) and (C) with the liquid velocity vectors; vapor velocities (not plotted) are always near-vertical (upwards). Phase regions are two-phase (VL), liquid (L) and vapor (V). Long dashed white lines indicate locations of the vertical cross-sections plotted in Figure 6. Dashed white lines in (E) and (F) bound the region where countercurrent flow takes place.

Two-phase heat-pipe systems develop when the bottom temperature is set close to, but slightly higher than, the boiling temperature for near-bottom pressures (Table 1, simulations 4,5,6,10,13,14,15,16). For $k = 5.0 \times 10^{-15} \text{ m}^2$, the aspect ratio ranges from 0.4 to 0.5 (Fig. 1). This type of convection is characterized by broad two-phase upflow zones, which are recharged at depth through heat-pipe mechanisms (Fig. 3E). At the center of the upflow zone, an ideal heat-pipe forms, with liquid and vapor flowing near-vertically in opposite directions. At the edges, liquid flows downward but also has a substantial horizontal flow component, so fluid flow is not truly countercurrent. The downward-flowing liquid phase boils off steadily, creating vapor that rises swiftly. This mechanism is very efficient in transferring energy and enables the formation of broad upflow zones (Fig. 3B) that can still be efficiently recharged. For $k = 5.0 \times 10^{-15} \text{ m}^2$, this convection style produces the largest Nu observed (up to 90).

For higher bottom temperatures (approximately 450°C or higher, i.e. Table 1, simulations 7,8,11,12,17,18), the system shifts toward two-phase vapor-dominated upflow zones that have substantially smaller and less ideal heat-pipe zones (Fig. 3C,F). These systems are characterized by small aspect ratios (approximately 0.33; Fig. 1), narrow upflow zones, and large pure-vapor regions directly above the bottom boundary (Fig. 3F). Nu values for two-phase

vapor-dominated convection are moderate, ranging from 10 to 20 for $k = 5.0 \times 10^{-15} \text{ m}^2$, with a trend toward slightly higher Nu for larger bottom temperatures.

Thus, Nu as a function of bottom temperature evolves from low values at single-phase conditions to a peak at two-phase heat-pipe conditions and toward moderate values at vapor-dominated conditions. This pattern is summarized in Fig. 4, which plots Nu against the temperature specified at the bottom boundary for the various

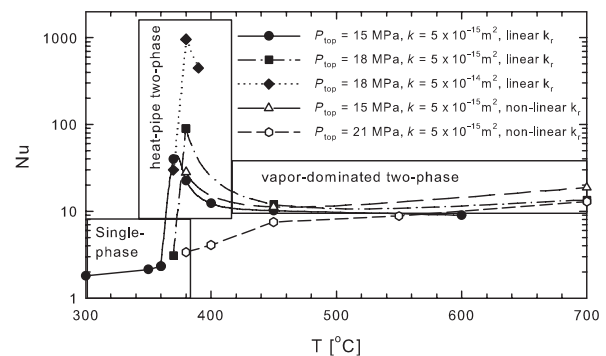


Fig. 4. Nusselt number (Nu) as function of bottom-boundary temperature for different top-boundary pressures, permeabilities and relative-permeability functions. Boxes indicate whether convection type was single-phase, two-phase heat-pipe or two-phase vapor-dominated. The dotted line connects simulations at supercritical conditions that are inherently single phase.

top-boundary-pressure, permeability and relative-permeability scenarios. It shows that high Nu can be reached when permeability is sufficient with several simulations close to $Nu = 100$ and some even close to $Nu = 1000$. The peak of maximum Nu shifts to higher temperatures when the top pressure is increased, reflecting the increased boiling temperature at higher pressures. Increasing the top pressure will increase Nu as long as bottom pressures do not exceed the critical pressure and thus eliminate two-phase flow. Two-phase fluids closer to the critical point will have a larger fluxibility, F , which is a measure of the ability of a fluid to transport energy (Jupp & Schultz 2000) and for a two-phase fluid is given by (Geiger *et al.* 2005):

$$F = \frac{k_{rl} S_l \rho_l}{\mu_l} (h_l - h_0) (\rho_0 - \rho_l) + \frac{k_{rv} S_v \rho_v}{\mu_v} (h_v - h_0) (\rho_0 - \rho_v). \quad (4)$$

Figure 5 illustrates the fluxibility of a two-phase fluid along the boiling curve for various volumetric liquid saturations. It shows that, for all pressure–temperature conditions, the vapor phase has a larger fluxibility than the liquid phase and that both increase toward the critical point. The maximum vapor fluxibility actually occurs at slightly lower pressure–temperature conditions than the critical point itself due to the larger specific enthalpy of the vapor at slightly subcritical conditions.

The drop in Nu from a peak at moderate bottom temperatures (370–400°C) toward substantially lower values at high bottom temperatures (450–700°C) is surprising and requires further explanation. We therefore analyze two

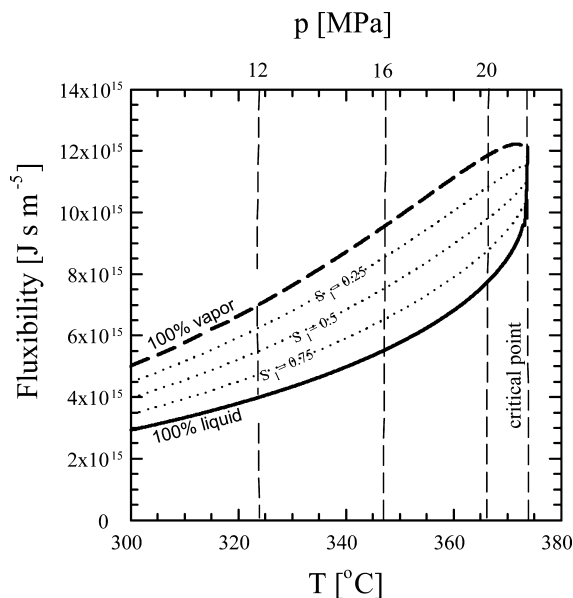


Fig. 5. Fluxibility (equation 4) along the boiling curve as a function of temperature, for different values of volumetric saturation. Vertical dashed lines indicate pressure along the boiling curve.

typical simulations in more detail. The first (Table 1, simulation 4) has standard conditions ($p_{\text{top}} = 15$ MPa and $k = 5.0 \times 10^{-15} \text{ m}^2$) with the bottom boundary set to 370°C. This simulation resulted in $Nu = 35$ and a snapshot is plotted in Fig. 3B. The second simulation (Table 1, simulation 8) is identical except for a bottom temperature of 600°C (snapshot in Fig. 3C). The second simulation resulted in a Nu of approximately 8 and lies within the vapor-dominated region in Fig. 4. The relatively low value of Nu results partly from the way Nu is calculated, because for a 600°C bottom temperature, the heat flux by conduction is larger. Still, its absolute energy transport is nearly three times smaller. Figure 6 shows fluid properties in vertical cross-sections through the upflow zone in the two simulations. It shows that the volumetric enthalpy ($S_l \rho_l h_l$) for the liquid phase is larger (Fig. 6D,H) and, as liquid saturations in the vapor-dominated simulation are smaller (Fig. 6A,E), the total volumetric enthalpy ($S_l \rho_l h_l + S_v \rho_v h_v$) is slightly smaller in the vapor-dominated case. In the top 300 m, liquid saturations in both simulations are similar (approximately 0.5 and approximately 0.4 respectively), such that the fluxibility of fluids in this part of the upflow zone is also similar. Therefore, a difference in fluid properties cannot account for the different amount of energy transported by the two simulations. However, because liquid saturations are below residual (0.3) in the bottom 200 m of the vapor-dominated case (Fig. 6E), countercurrent flow paths cannot develop here. In fact, only a very narrow zone at the edge of the two-phase area shows countercurrent flow (Fig. 3F). The low density of the vapor phase precludes the formation of a stable horizontal vapor layer at the bottom, resulting in many narrow upflow zones. In contrast, in the simulation with lower bottom temperature, the region where vapor and liquid flow in opposite directions is much larger (Fig. 3E). The heat-pipe mechanism efficiently recharges the root of the hydrothermal upflow zone and thereby allows the formation of a broad upflow zone. Therefore, upflow occurs in a horizontal surface area roughly three times larger in this simulation than in the vapor-dominated one (compare Fig. 3B,C). This results thus in larger total mass fluxes – and therefore energy fluxes – through the system.

If bottom pressures exceed the critical pressure, single-phase supercritical flow develops (Table 1, simulations 19–23) and results in Nu similar to vapor-dominated systems (Fig. 4). Supercritical convection at $5.0 \times 10^{-15} \text{ m}^2$, with bottom temperatures set to 450–550°C, is characterized by aspect ratios approximately 0.35 and Nu of approximately 7.5–9.0. Buoyancy forces in supercritical systems are smaller than those in boiling systems, and countercurrent fluid flow cannot develop. Figure 7 compares the pressure in upflow and downflow regions with hydrostatic pressures, for subcritical (18 MPa at the top) and supercritical (21 MPa at the top) systems with bottom temperatures of 450°C. It shows that driving forces are much larger in the subcritical case,

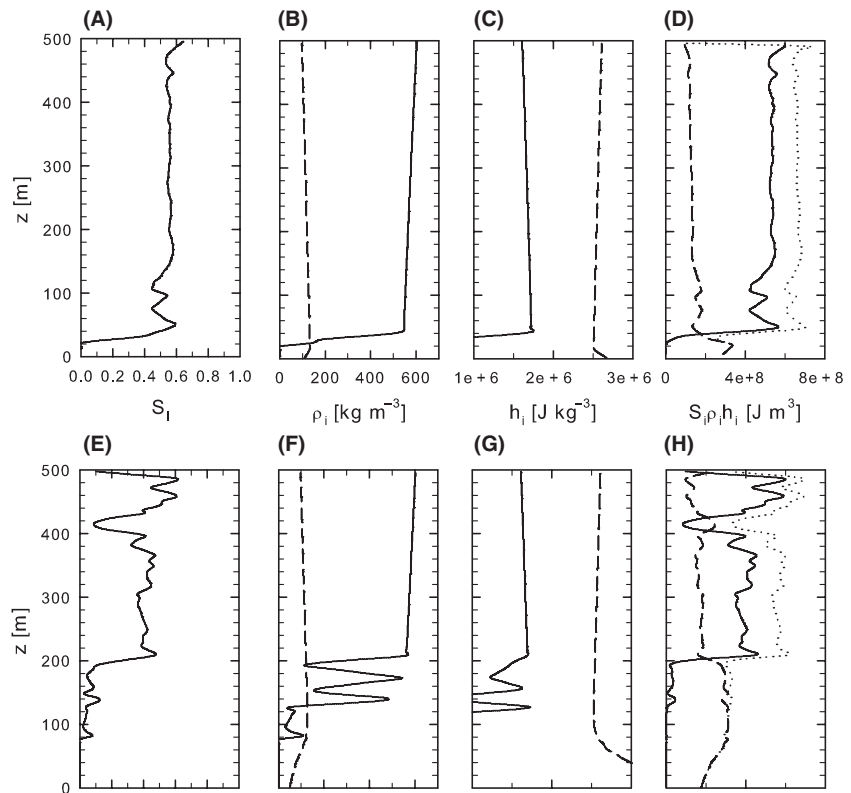


Fig. 6. Liquid (solid) and vapor (dashed) properties in the upflow zone of a two-phase heat-pipe simulation (Fig. 3b): (A) liquid saturation, (B) density, (C) specific enthalpy and (D) volumetric enthalpy, where the dotted curve in (D) is the sum of liquid and vapor; and in the upflow zone of two-phase vapor-dominated simulation (Fig. 3c) (E–H).

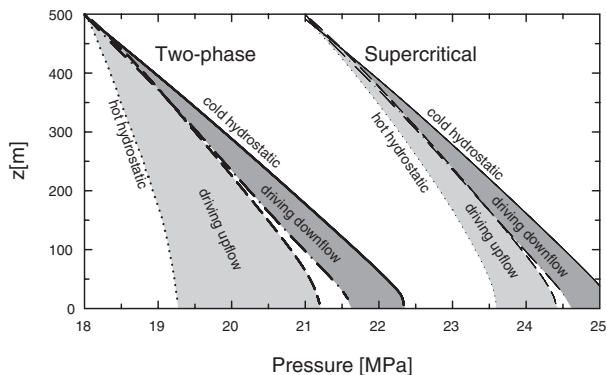


Fig. 7. Pressure-depth distribution in upflow zone (dashed) and downflow zone (dash-dotted) of a two-phase system (18 MPa at top) and a supercritical system (21 MPa at top), relative to hydrostatic pressure values derived from the fluid density distribution in the upflow (dotted) and downflow (solid) zone.

due to the density-lowering effect of the vapor phase. In simulation 23 (Table 1), in which k was set to $5.0 \times 10^{-15} \text{ m}^2$, the top pressure to 21 MPa and the bottom temperature to 700°C , rising supercritical fluids hit the critical point and follow the boiling curve from that point upward (Fig. 2). However, this simulation produced only moderate Nu of approximately 13.

In three simulations, an order-of-magnitude higher permeability was used, $5.0 \times 10^{-14} \text{ m}^2$, producing Nu of

up to approximately 1000. We also tested the effect of nonlinear Brooks–Corey type relative-permeability functions (Brooks & Corey 1964). The use of nonlinear relative permeabilities (Table 1, simulations 16–18) did not affect the Nu -curve as a function of temperature substantially (Fig. 4).

DISCUSSION

Energy transport in near-critical boiling hydrothermal systems under conditions and geometries resembling those in mid-ocean ridge settings is affected by several factors that interact nonlinearly, influencing the efficiency of convective systems to transport energy. These may be qualitatively summarized as follows:

- (1) Two-phase fluids close to the critical point have a larger fluxibility than fluids at lower pressure and temperature, indicating their enhanced ability to transport energy.
- (2) The presence of vapor in two-phase systems increases the variability in fluid density and thereby increases buoyancy forces in comparison to single-phase systems. This can increase energy efficiency.
- (3) Two-phase heat-pipes are efficient energy-transfer mechanisms and, specifically, enable the formation of broad upflow zones. Their impact decreases at pressures closer to the critical point, where the density and enthalpy of the liquid approach the density and enthalpy of the vapor phase.

- (4) The formation of (near) 100% vapor zones below two-phase upflow zones immobilizes the liquid phase, so that zones of countercurrent flows become small and broad upflow zones cannot form. This reduces the efficiency of energy transport.

These four factors interact with each other, sometimes having opposing effects, to form convection patterns and associated energy fluxes that vary highly nonlinearly with pressure–temperature boundary conditions. This leads, for instance, to the counterintuitive effect that applying higher temperatures at the bottom can decrease the efficiency of a system to transport energy.

The findings of this study have implications for the occurrence of ‘superconvective’ systems, i.e. systems with $Nu > 100$, in nature. We were able to produce superconvection at relatively low permeability, indicating that superconvection might be more common than previously thought (Ingebritsen & Hayba 1994). However, the conditions under which superconvection occurred were very restricted; for instance, overly hot bottom temperatures reduce energy transport. Thus it remains to be seen if such conditions are widespread in nature. In fact, a possible run-away effect could play a role: if a superconvecting two-phase heat-pipe would, by external forces, be heated to higher bottom temperatures, then its efficiency would drop, increasing bottom temperatures even more. The temperature at which cooling rock becomes permeable could also potentially have an effect on the occurrence of two-phase superconvection. If this transition occurs at high temperatures, then two-phase superconvection at moderate permeability seems unlikely.

Nevertheless, this study shows that near-critical two-phase convection, facilitated by heat-pipe mechanisms, can transport energy very efficiently. The impact of heat-pipes could be even more significant in nature, because the top boundary condition in our models precluded the formation of heat-pipes at the top – fluid flow at the top was allowed to be either up or down, but not countercurrent.

For computational reasons, we used relatively moderate permeabilities in this study. At mid-ocean spreading centers permeability is likely to be higher by an order of magnitude or more (Fisher 1998; Lowell & Germanovich 2005), which could push Nu to larger values. In addition, the presence of salt in seawater allows phase-separation at pressures well above the critical region, possibly broadening the range of conditions where heat-pipes can form. However, the effect of salt on our results is hard to anticipate, as double-diffusive double-advective convection will also occur when salt is present (Geiger *et al.* 2005). Also, the possible formation of static brine layers near the bottom could have an insulating effect, reducing the energy transport (Kawada *et al.* 2004). Further numerical studies are required to investigate the effects of these issues.

CONCLUSIONS

Simulations of two-phase flow of pure water at near-critical conditions show that, under restricted conditions, two-phase phenomena can greatly enhance energy transport by convection. The possibility of countercurrent flow gives an additional degree of freedom allowing convection cells to attain a state of optimum energy transport. This way, broad upflow zones can form, with roots recharged by heat-pipe mechanisms that are highly efficient in transporting energy. Due to the restricted conditions under which they can form, it remains to be seen if such high-heat-flux systems exist in nature.

ACKNOWLEDGEMENTS

The authors like to thank Steve Ingebritsen, Philipp Weiss, Shaul Hurwitz and an anonymous reviewer for their helpful comments which have considerably improved the manuscript. Funding was provided by the Swiss National Science Foundation, grant number 200020-107955.

REFERENCES

- Bai WM, Xu WY, Lowell RP (2003) The dynamics of submarine geothermal heat-pipes. *Geophysical Research Letters*, **30**, 1–4.
- Brooks RH, Corey AT (1964) Hydraulic properties of porous media. *Hydrological Papers*, Vol. 3. Colorado State University, USA.
- Cathles LM (1977) An analysis of the cooling of intrusives by ground-water convection which includes boiling. *Economic Geology*, **72**, 804–26.
- Coumou D (2008) *Numerical simulation of fluid flow in mid-ocean ridge hydrothermal systems*. PhD Thesis, ETH Zurich, Switzerland.
- Coumou D, Driesner T, Geiger S, Heinrich CA, Matthai S (2006) The dynamics of mid-ocean ridge hydrothermal systems: splitting plumes and fluctuating vent temperatures. *Earth and Planetary Science Letters*, **245**, 218–31.
- Cox BL, Pruess K (1990) Numerical experiments on convective heat-transfer in water-saturated porous-media at near-critical conditions. *Transport in Porous Media*, **5**, 299–323.
- Dunn JC, Hardee HC (1981) Superconvecting geothermal zones. *Journal of Volcanology and Geothermal Research*, **11**, 189–201.
- Fisher AT (1998) Permeability within basaltic oceanic crust. *Reviews of Geophysics*, **36**, 143–82.
- Fontaine FJ, Wilcock WSD (2007) Two-dimensional numerical models of open-top hydrothermal convection at high Rayleigh and Nusselt numbers: Implications for mid-ocean ridge hydrothermal circulation. *Geochemistry Geophysics Geosystems*, **8**, Q07010, doi:10.1029/2007GC001601.
- Fournier RO (1999) Hydrothermal processes related to movement of fluid from plastic into brittle rock in the magmatic-epithermal environment. *Economic Geology and the Bulletin of the Society of Economic Geologists*, **94**, 1193–211.
- Geiger S, Driesner T, Heinrich CA, Matthai SK (2005) On the dynamics of NaCl–H₂O fluid convection in the Earth’s crust. *Journal of Geophysical Research – Solid Earth* **110**, 1–23.

- Haar L, Gallagher JS, Kell GS (1984) *NBS/NRC Steam Tables*. Hemisphere Publishing Corporation, Washington, New York, London.
- Hayba DO, Ingebritsen SE (1997) Multiphase groundwater flow near cooling plutons. *Journal of Geophysical Research*, **102**, 12235–52.
- Heinrich CA, Driesner T, Stefánsson A, Seward TM (2004) Magmatic vapor contraction and the transport of gold from the porphyry environment to epithermal ore deposits. *Geology*, **32**, 761–4.
- Hurwitz S, Kipp KL, Ingebritsen SE, Reid ME (2003) Groundwater flow, heat transport, and water table position within volcanic edifices: implications for volcanic processes in the Cascade Range. *Journal of Geophysical Research – Solid Earth* **108**, B12, 1–19.
- Ingebritsen SE, Hayba DO (1994) Fluid-flow and heat-transport near the critical-point of H₂O. *Geophysical Research Letters*, **21**, 2199–202.
- Ingebritsen SE, Sanford W, Neuzil C (2006) *Groundwater in Geologic Processes*. Cambridge University Press, Cambridge.
- Jupp T, Schultz A (2000) A thermodynamic explanation for black smoker temperatures. *Nature*, **403**, 880–3.
- Jupp TE, Schultz A (2004) Physical balances in seafloor hydrothermal convection cells. *Journal of Geophysical Research – Solid Earth*, **109**, B5, 1–12.
- Kawada Y, Yoshida S, Watanabe S (2004) Numerical simulations of mid-ocean ridge hydrothermal circulation including the phase separation of seawater. *Earth Planets and Space*, **56**, 193–215.
- Lowell RP, Germanovich L (2005) Hydrothermal processes at mid-ocean ridges: results from scale analysis and single-pass models. In: *Hydrothermal Interactions between the Lithosphere and Oceans*, vol. 148 (eds German CR, Lin J, Parson LM). pp. 219–244. Geophysical Monograph, American Geophysical Union, Washington DC, USA.
- McGuinness MJ (1996) Steady solution selection and existence in geothermal heat-pipes .1. The convective case. *International Journal of Heat and Mass Transfer*, **39**, 259–74.
- McGuinness MJ (1997) Steady-solution selection and existence in geothermal heat-pipes .2. The conductive case. *International Journal of Heat and Mass Transfer*, **40**, 311–21.
- McGuinness MJ, Blakeley M, Pruess K, Osullivan MJ (1993) Geothermal heat-pipe stability – solution selection by upstreaming and boundary-conditions. *Transport in Porous Media*, **11**, 71–100.
- Norton D, Knight J (1977) Transport phenomena in hydrothermal systems – cooling plutons. *American Journal of Science*, **277**, 937–81.
- Schubert G, Straus JM (1977) 2-Phase convection in a porous-medium. *Journal of Geophysical Research*, **82**, 3411–21.
- Schubert G, Straus JM (1979) Steam-water counterflow in porous-media. *Journal of Geophysical Research*, **84**, 1621–8.
- Schubert G, Straus JM (1980) Gravitational stability of water over steam in vapor-dominated geothermal systems. *Journal of Geophysical Research*, **85**, 6505–12.
- Seyfried WE, Seewald JS, Berndt ME, Ding K, Foustoukos DI (2003) Chemistry of hydrothermal vent fluids from the Main Endeavour Field, northern Juan de Fuca Ridge: geochemical controls in the aftermath of June 1999 seismic events. *Journal of Geophysical Research – Solid Earth*, **108**, B9, 1–23.
- Straus JM, Schubert G (1977) Thermal-convection of water in a porous-medium – effects of temperature-dependent and pressure-dependent thermodynamic and transport properties. *Journal of Geophysical Research*, **82**, 325–33.
- Von Damm KL, Lilley MD, Shanks WC, Brockington M, Bray AM, O'Grady KM, Olson E, Graham A, Proskurowski G (2003) Extraordinary phase separation and segregation in vent fluids from the southern East Pacific Rise. *Earth and Planetary Science Letters*, **206**, 365–78.